Electron spin resonance characterization of a divacancy-related centre in CVD diamond

2000 J. Phys.: Condens. Matter 12 7807

(http://iopscience.iop.org/0953-8984/12/35/315)

J. Phys.: Condens. Matter **12** (2000) 7807–7817. Printed in the UK PII: S0953-8984(00)14640-5

Electron spin resonance characterization of a divacancy-related centre in CVD diamond

A Stesmans, B Nouwen and K Iakoubovskii
Department of Physics, University of Leuven, Celestijnenlaan 200D, 3001 Leuven, Belgium

Received 12 June 2000

Abstract. The electron spin resonance characterization of an undocumented paramagnetic centre in chemical vapour deposited diamond is reported. Successful fitting of the powder pattern-like spectrum characterized the originating defect as an $S = 1$ centre of spectroscopic splitting factor $g = 2.003\,86 \pm 0.000\,05$. The zero-field splitting parameters were determined as $D = 358 \pm 1$ G and $E = 0 \pm 2$ G at 294 K. Two hyperfine spectra were resolved, one ascribed to four equivalent C sites. Various suggestions as to the microscopic nature of the defect are explored. The centre is suggested to be an impurity stabilized divacancy-like defect.

1. Introduction

Vacancy-related centres in diamond have been extensively studied by electron spin resonance (ESR) over the last decades. Several excellent reviews on the subject have been presented [1–3]. The single vacancy in diamond forms a tetrahedral centre with effective spin $S = 5/2$, 0 and $1/2$ in the negative, neutral and positive charge states, respectively [4]. It can be created by irradiation (e.g. electrons, ions, neutrons), by plastic deformation or by heat. Annealing at 600 °C or higher temperatures results in the diffusion of the vacancies and appearance of different vacancy-related complexes. Often, this process is accompanied by trapping of nitrogen, the dominant impurity in most types of diamond, commonly resulting in the formation of nitrogen–vacancy (N–V) aggregates with up to four N atoms (xN–V; $x = 1, \ldots, 4$) [2]. Apart from these, several tens of other complexes containing one or more vacancies are known from ESR studies [1]. However, the microscopic structure of most of them still remains obscure.

In relatively pure (IIa type) diamond, post-irradiation annealing at 800 °C results in aggregation of vacancies into divacancies. The structure of the divacancy, as recently determined by an ESR study on crystalline diamond [5], appears to be very similar to the divacancy in Si [6]. At low temperature, four out of six dangling bonds surrounding the divacancy pair off. The remaining two bond electrons form an $S = 1$ paramagnetic state of C_{2h} symmetry. An increase in temperature from 30 to 300 K results in a gradual transition from the C_{2h} to the D_{3d} symmetry due to thermally activated hopping between different orientations. The divacancy in diamond has some unexpected features. Among others, and in contrast with the Si-divacancy case, the number of nearest neighbour (NN) atoms as determined from ESR hyperfine interaction observations is not two but four. Also, the value of the spin–spin coupling constant (see below for details) $D = 166$ G at 33 K, when no reorientation occurs yet, is significantly smaller than the value $D \sim 470$ G, calculated within a point dipole approximation for two electrons at a divacancy site [1]. The discrepancy is attributed to delocalization of

0953-8984/00/357807+11$30.00

the interacting electrons. The observed anisotropy of the D-matrix is consistent with this explanation.

Defects in diamond have majorly been studied on natural and synthetic crystals. The progress in the growth of diamond by chemical vapour deposition (CVD) resulted in a shift of the focus towards CVD films. Several peculiarities of the growth process strongly promote defect formation in CVD diamond. CVD films are typically synthesized from a 99:1 H_2:CH_4 mixture and, therefore, contain a lot of hydrogen. Most of the hydrogen atoms in CVD diamond probably form C–H bonds, whose concentration can be estimated from infrared (IR) absorption measurements, giving a typical result of 100–1000 ppm [7]. The presence of oxygen and nitrogen in the growth mixture is partly determined by leaks into the CVD chamber. Therefore, nominally undoped films often contain these elements. Oxygen is known to form IR-active C=O and C–O–C groups at the surface of the CVD film [8], while nitrogen is mostly incorporated as single substitutional centres or as N–V complexes [9].

The non-thermodynamic nature of the growth process results in the generation of a large number of vacancies. They are not stable at the typical growth temperature (700–900 °C) and tend to be trapped by various impurities. The hydrogen–vacancy (H–V) centre ($S = 1/2$) produces a characteristic ESR signal with a broad (4–8 G) line at $g = 2.0028$ and two weaker satellites, which were shown to originate from the forbidden spin-flip hyperfine interaction of a carbon dangling bond electron with a hydrogen atom on a nearest-neighbour C–H [10]. In accordance with the theory, the intensity of these satellites is proportional to the inverse square of the microwave frequency ν, while the splitting linearly increases with the frequency. It was shown that the H–V centre preferentially resides in stressed regions near grain boundaries, and therefore ESR lines from this centre are broad, even in high-quality CVD films [10]. ESR lines from the H–V centre change their amplitudes after annealing at temperatures above 1200 °C, ascribed to hydrogen rearrangement due to dissociation of C–H bonds [7].

The nitrogen–vacancy (N–V) is a trigonal defect. In its negative state, it has been thoroughly characterized by different resonance techniques [2]. It forms an $S = 1$ centre with $g = 2.0028$ and $D = 1027$ G [1]. Although predicted to have spin 1/2, the N–V centre in its neutral state has not yet been detected by ESR [2].

While several centres involving one vacancy are known in CVD diamond, no divacancy-related complexes have been identified yet. In the present paper we report on the ESR characterization of an undocumented spectrum in CVD diamond, which is assigned to a divacancy-like complex, possibly stabilized by the presence of an impurity.

2. Experimental details

2.1. Sample preparation

Undoped and nitrogen-doped diamond films were grown on Si substrates in an ASTeX PDS-17 microwave plasma reactor [11], typically using a microwave power of 5 kW and a gas flow rate of 300 cm^3 min^{-1}, with the substrate temperature held at 800 °C. Nitrogen doping was obtained by adding up to 0.1% of N_2 to the feed gas mixture. After film deposition, the substrates were removed by chemical etching, leaving unoriented polycrystalline films with grain sizes in the range 0.5–5 μm.

The impurity content of the samples was investigated by means of Rutherford backscattering spectroscopy (RBS). The measurements revealed the presence of up to 1% of elements with mass number 59 ± 4 and 96 ± 4. Other impurities remained undetectable (<0.1%). The occurrence of these impurities is attributed to plasma etching of the stainless steel reactor wall during the CVD process. Particularly Fe, Ni and Mo could thus be

incorporated. Further experimental details on the sample preparation and characterization have been described previously [9].

2.2. ESR spectroscopy

Most of the ESR measurements were carried out using a commercial Q-band ($\nu \sim 34$ GHz) reflection spectrometer (Bruker EMX) driven in absorption mode under conditions of adiabatic slow passage. The measurement temperature T could be varied in the range 10–300 K. The spectrometer set-up allows modulation of the applied external field $\boldsymbol{B}$ at 100 kHz, resulting in the detection of absorption derivative spectra $\mathrm{d}P_\mu/\mathrm{d}B$. Here, P_μ represents the applied microwave power to the cylindrical TE_{011} cavity (typical loaded quality factor of 1500–3000).

Special care was taken to avoid spectroscopic distortion due to saturation and/or overmodulation. To enhance the signal-to-noise ratio, the spectrometer signal averaging capabilities were extensively used: typically up to several hundred field scans were added. A comounted calibrated marker sample, i.e. $MgO:Cr^{3+}$ ($g = 1.979\,60 \pm 0.000\,02$, $S = 1/2$), calibrated against the LiF standard [12], was used as intensity and magnetic field value reference. Spin densities were determined by comparison of the signal intensities (the area under the absorption curve) as generally obtained by double numerical integration of the experimental spectra. However, for broad spectra (>100 G), where unambiguous determination of the baseline appeared troublesome, optimized simulated spectra were integrated. Additional ESR observations were carried out using a home built K-band ($\nu \sim 20.5$ GHz) spectrometer described elsewhere [13].

3. Experimental results

Figure 1 shows a typical Q-band ($\nu = 33.607$ GHz) ESR spectrum measured at 293 K. The spectrum consists of a broad resonance signal (cf α in figure 1(B)) of a zero crossing g value $g = 2.002\,79 \pm 0.000\,05$, accompanied by a doublet in the wings of 40.0 ± 0.5 G splitting. These satellites exhibit a characteristic behaviour with ν: at $\nu = 20.5150$ GHz the splitting decreases to 26 ± 1 G, while the intensity relative to the central line increases noticeably. This signal was previously ascribed to the H–V centre [10].

Several relatively weaker signals appear to be superimposed on the intense central line. In the $g = 2.0048$–2.0053 region a two-peak structure (denoted β in figure 1(B)) of total width $\sim$1.7 G is present. The structure is reminiscent of the powder pattern-like structure of a defect with an axial g matrix like, e.g. the E′ defect in SiO_2 [14], with $g_\parallel = 2.005\,15 \pm 0.000\,10$ and $g_\perp = 2.004\,90 \pm 0.00010$. Another resonance line (cf γ in figure 1(B)) of peak-to-peak width $\Delta B_{pp} = 0.67 \pm 0.10$ G is observed at $g = 2.004\,30 \pm 0.000\,05$. Finally, on the negative lobe of the central structure, a single small line (denoted δ in figure 1(B)) of $\Delta B_{pp} \approx 0.3$ G is observed at $g = 2.002\,12 \pm 0.000\,05$. Possibly, this line could form a single spectrum together with two very weak (not well exposed in figure 1) features appearing on the steep slope near the zero crossing at $g \approx 2.002\,41$ and $g \approx 2.002\,72$: they appear equidistant with a spacing of 1.7 ± 0.3 G within experimental error. Being superposed on the central line structure, the correct spectroscopic assessment of all these small-intensity lines, however, is much hampered.

Of more interest, here, is that in the remote wings of the central signal, a doublet of very characteristic asymmetric lines (a in figure 1(A)) of 358 ± 1 G splitting is observed, together with one more, much weaker, doublet of absorption-like shape with a splitting exactly twice as large (cf b in figure 1(A)). The latter two doublets are centred at $g = 2.003\,86 \pm 0.000\,05$,

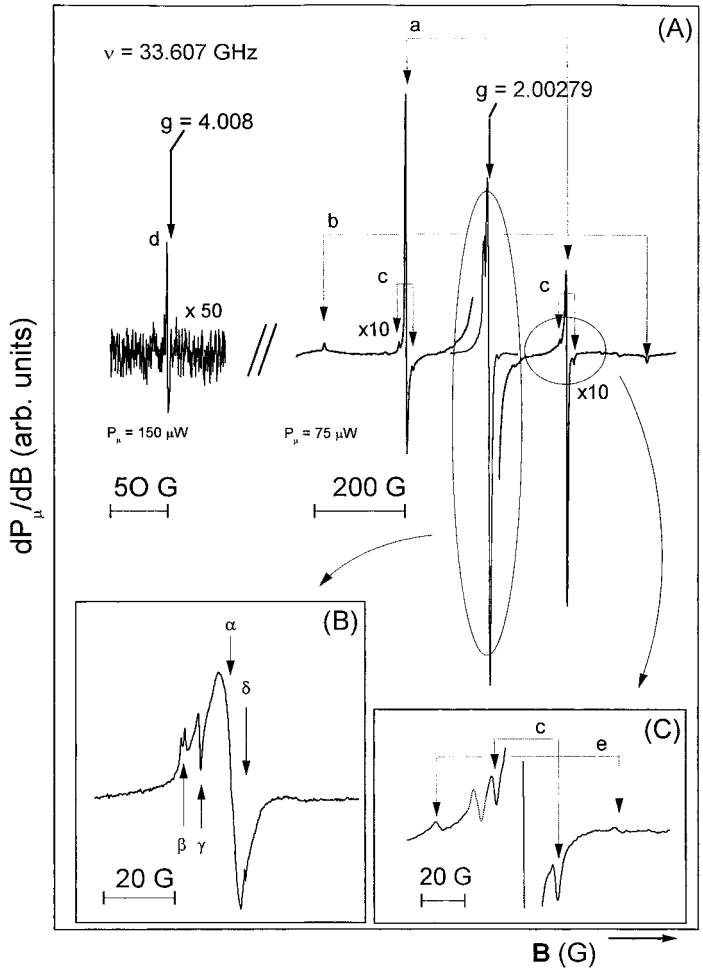

Figure 1. An example of the discussed ESR absorption derivative spectrum, observed in CVD diamond using a Q-band spectrometer at room temperature. The insets show magnifications of the indicated regions. The doublet structures a and b represent powder pattern features of an $S = 1$ state. Line d is attributed to a $\Delta m = 2$ transition of the same centre. The resonances marked c are identified as due to hyperfine interaction. The weak lines indicated by e might be traces of additional hyperfine interaction, though their origin is uncertain. Inset (B) shows that the broad central line is a superposition of several lines. Mark α labels the major central line, while β, γ and δ indicate observed additional structure. The dotted resonance line in the right inset (C) is part of a sextet background signal.

that is, slightly left from the central structure. Furthermore, around each of the 358 G doublet peaks, another weak pair of satellites (doublet c in figure 1(C)) is observed with a splitting of 28.3 ± 0.3 G, exhibiting the same asymmetrical shape and peak-to-peak width as the doublet lines a. Finally, though very weak, another narrow asymmetrical line (marked d in figure 1(A)) of width $\Delta B_{pp} = 0.7 \pm 0.1$ G is observed in the half-field region at $g = 4.008$. At K-band frequency (20.5 GHz) the width increases to $\Delta B_{pp} = 2.1 \pm 0.2$ G.

Through optimization of the spectrometer setting and intense signal averaging, much effort was given to detect additional signals, particularly in the region around each of the weak 716 G doublet lines, without success however. Yet, in the neighbourhood of the 358 G doublet

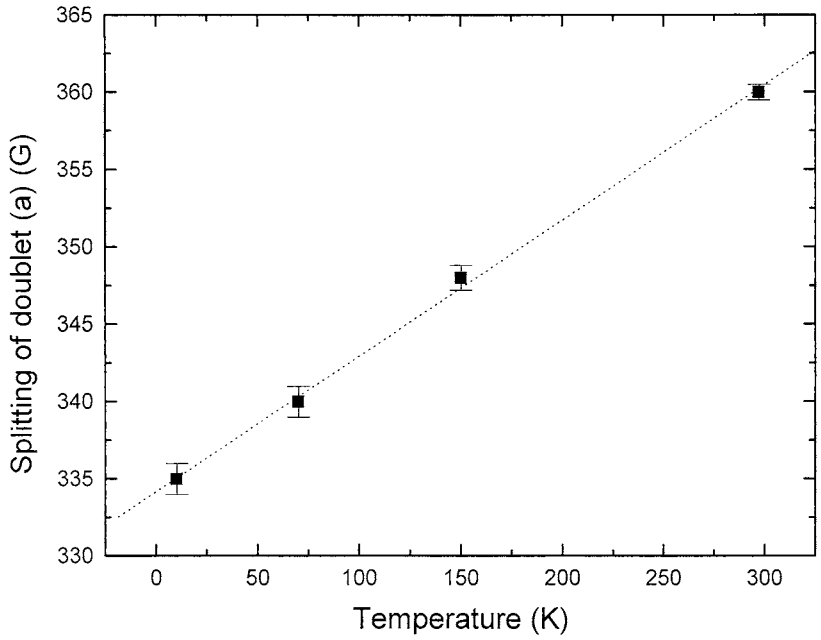

Figure 2. Temperature dependence of the splitting of doublet (a) (measure of spin–spin coupling constant D) (cf figure 1(A)).

lines, more weak signal-like features did show up reproducibly. Remarkable is the occurrence of two very weak signals almost perfectly centred—as if they were hyperfine lines—on the high-field 358 G doublet line with a splitting of 88 ± 1 G (cf doublet e, figure 1(C)). Though of comparable magnitude, the influence of noise makes it very difficult to judge whether the intensities of both signals are equal. They are estimated at $14 \pm 5\%$ of the intensity of each of the 28 G doublet c lines. No additional lines of comparable intensities could be discerned. It should be added, though, that some lines could be masked by the occurring (larger-intensity) resonance lines. Furthermore, observation of an equivalent doublet on the low-field side of the spectrum failed, likely because of strong interference of cavity background signals. Also, their observation at the K-band failed.

The observational temperature T affects both the spectrum width and saturability. Avoiding saturation effects at room temperature required the incident microwave power P_μ to be reduced to below ~ 5 μW. Even at these power levels some slight effects of saturation—negligible for the current investigation, though—were observed in the central line structure. At 70 K, significant saturation could not be avoided for $P_\mu \sim 1$ μW, the minimum power required for stable operation of the Q-band spectrometer during signal averaging. Upon cooling, an apparently linear decrease in the splitting of the 358 G doublet is observed, as shown in figure 2, the separation varying as $334.2 + 0.0877T$(K). No angular dependence could be observed confirming that no significant preferential orientations are present in the sample.

Surprisingly, the spectrum under investigation, i.e. the described structures apart from the central part, could be observed in only three samples out of several tens studied. A closer analysis revealed that this spectrum is absent if lines due to substitutional nitrogen [1] are present. The three samples displaying the above spectrum exhibit an exceptionally low nitrogen content. This anticorrelation of the newly observed spectrum with the spectrum of the substitutional nitrogen centre is demonstrated in figure 3(a), where the ratio of the

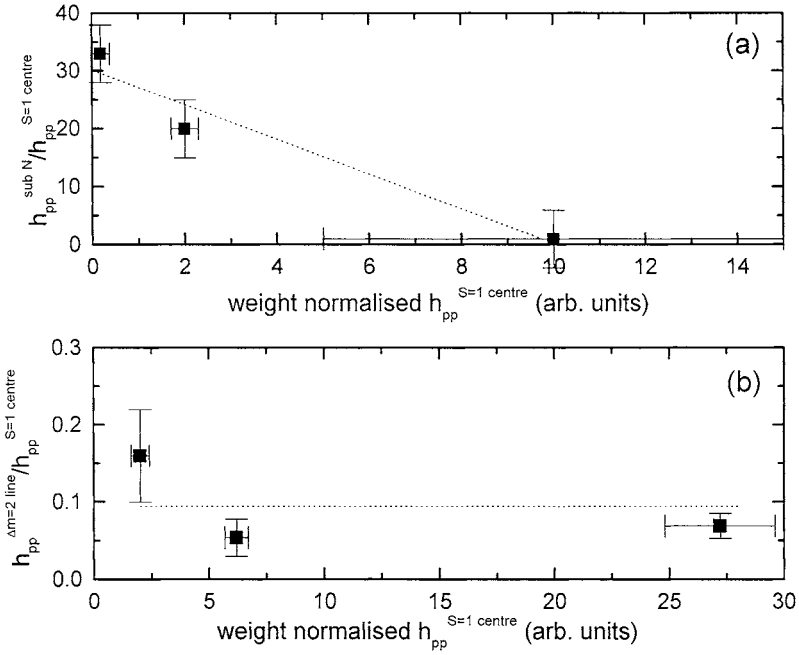

Figure 3. Relative peak-to-peak height of the substitutional nitrogen centre (a) and the $\Delta m = 2$ transition (b) as function of the peak-to-peak height, normalized to the sample weight, of the observed $S = 1$ centre. Dotted lines indicate trends.

characteristic peak-to-peak height of the substitutional nitrogen centre $h_{pp}^{sub\,N}$ to one of the currently investigated centres, designated $h_{pp}^{S=1}$, is plotted as a function of the weight normalized $h_{pp}^{S=1}$, indicative of the spin density.

Annealing treatments at 1000 °C for 2 h in 10^{-5} Torr vacuum did not affect the investigated spectrum, while further annealing at 1400 °C for 2 h in 10^{-8} Torr vacuum resulted in a $\sim$3 times increase of the signal intensity. If admitting an effective spin $S = 1$ for the currently investigated defect (see below for details), the maximum density thus observed is estimated at $(1.6 \pm 0.5) \times 10^{16}$ spins g^{-1}. The latter count is based on comparison of the intensities of the signal under investigation and the marker, by using idealized line shape relations as obtained from simulations (see below for details) and taking into account the different spin properties of both systems, in the manner presented in [15].

4. Simulation and analysis

The whole set of ESR lines described above, apart from the composed central structure, can be excellently simulated as a powder pattern spectrum of a single defect centre. The simulation was carried out using an algorithm based on second order perturbation theory to calculate the eigenvalues of the underlying Hamiltonian. The generation of powder pattern line shapes requires averaging of the eigenvalues over many orientations with respect to the field. In the present case 800 × 800 points per hemisphere were standardly used. This choice proved large enough to ensure that the calculated spectra were independent of averaging. No 'glass effect' was introduced. Besides the broadening contributions due to the powder effect, various other broadening mechanisms, e.g. due to strain, finite relaxation time, unresolved hyperfine

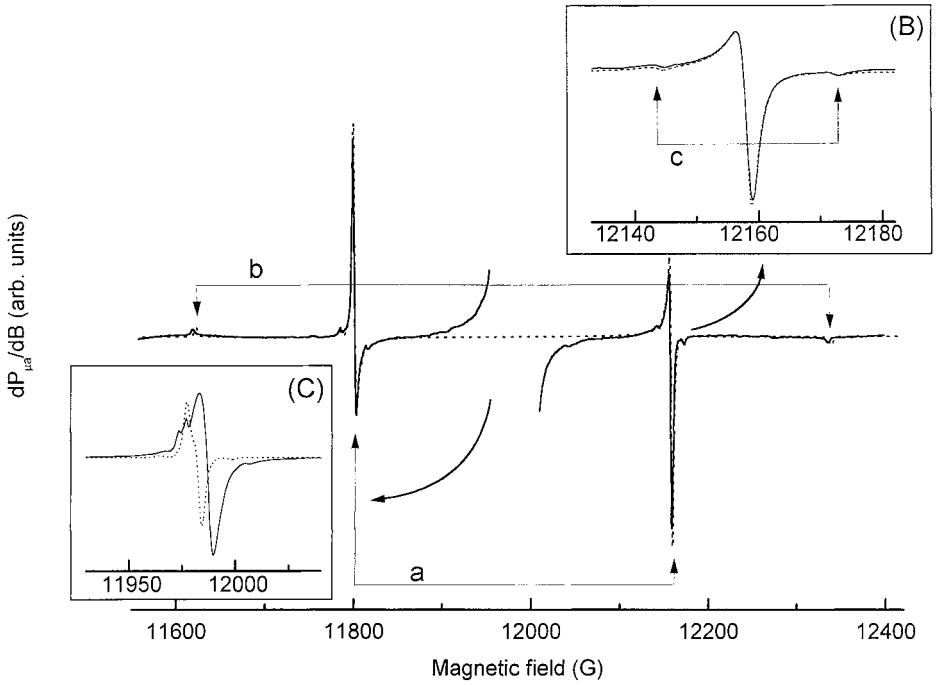

Figure 4. Optimized fitting (thick dotted curve) of the newly observed experimental (thick solid curves) spectrum. The upper right inset (B) shows a magnification of the indicated part of the spectrum, exposing the additional hyperfine doublet, which is also observed around the low-field part of doublet a. The dotted curve here represents a fit assuming isotropic hf interactions with one $I = 1/2$ nucleus. The simulations were carried out assuming $S = 1$, and the intensity ratio of the hyperfine lines to the total spectrum was chosen to be 4.4%. The bottom left inset (C) compares the observed central lines (full curve) for a fit assuming $S = 3/2$ (dotted curve), indicating the inadequacy of the $S = 3/2$ model.

etc, might be involved. These are incorporated by convoluting the powder pattern with a representative 'single crystal' shape function line, for which the best choice was found to be a Lorentzian line of $\Delta B^R_{pp} = 1.75 \pm 0.05$ G.

The simulation is based on the spin Hamiltonian

$$\boldsymbol{H} = \beta \boldsymbol{S} \cdot \hat{g} \cdot \boldsymbol{B} + \boldsymbol{S} \cdot \hat{D} \cdot \boldsymbol{S} + \boldsymbol{S} \cdot \hat{A} \cdot \boldsymbol{I} \tag{1}$$

where the first term describes the classical Zeeman interaction of a system of effective spin $\boldsymbol{S}$ with the applied magnetic field B via the spectroscopic splitting dyadic $\hat{g}$, and β represents the Bohr magneton. The second term accounts for the fine-structure spin–spin interaction when $S > 1/2$. This term is often expressed in terms of the zero-field splitting parameters $D \equiv \frac{3}{2}D_3$ and $E \equiv \frac{1}{2}(D_1 - D_2)$, where D_1, D_2 and D_3 represent the respective elements of the diagonalized traceless matrix $\hat{D}$. The last term in expression (1) represents the hyperfine (hf) interaction of the spin $\boldsymbol{S}$ with the nuclear spin $\boldsymbol{I}$ of surrounding nuclei via the hf coupling tensor $\hat{A}$.

Fitting of the experimental spectrum applying the above Hamiltonian (1) to an ensemble of randomly oriented defects (powder pattern) bears out, reliably, that S needs to be either 1 or $3/2$, with an isotropic spectroscopic splitting factor $g = 2.003\,86 \pm 0.000\,05$. Figure 4 shows spectra (dashed curves) obtained along both interpretations, illustrating an almost perfect fit to the main spectrum composed of doublets a and b. For the case $S = 1$, $\hat{D}$ exhibits cylindrical

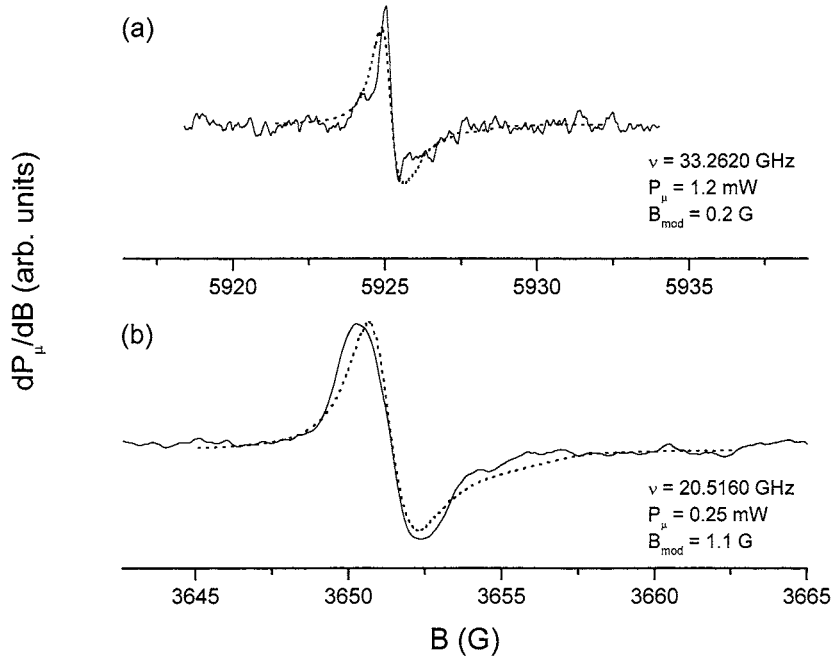

Figure 5. Comparison of calculated half field lines (dotted curves) to the newly observed experimental ones (solid lines) for the Q- (a) and K-band measurements (b) carried out at 300 K. Calculations were carried out assuming the lines to be $\Delta m = 2$ transition powder pattern spectra originating from an axially symmetric $S = 1$ paramagnetic state characterized by zero-field splitting parameter $D = 358$ G.

symmetry with $E = 0 \pm 2$ G and $D = 358 \pm 1$ G, while for $S = 3/2$, $D = 178.5 \pm 1.0$ G, i.e. half the value for $S = 1$. Both interpretations for the Hamiltonian allow equally good fitting of the 358 G and 716 G doublet structure (a and b in figure 4 respectively). The only difference between both calculated spectra is the presence of an intense central line structure in the $S = 3/2$ case, as shown (dashed curve) in inset (C) of figure 4.

The presence of the 28 G doublets ((C) in figures 1 and 4) around each of the lines of splitting 358 G is incorporated in the simulated spectra by assuming hf interaction of the electron spin with surrounding nuclei. Here, it is important to notice that, if an hf interaction is present, the x and y components of the hf interaction are responsible for occurring hf doublets around each of the 358 G splitted lines, while the z component manifests itself as a doublet symmetrically around each of the 716 G splitted doublet lines. Apparently, the latter hf component has remained undetected. This is well accounted for by the simulations, indicating that these lines would remain buried in the noise. Assuming isotropic hf interaction, with one $I = 1/2$ nucleus, a satisfactory fit (dotted curve) may be obtained, as shown by the enlarged view in inset (B) of figure 4, from where the ratio of the intensities of the total hf spectrum and the main spectrum was taken as 4.4%. Optimum fitting gives for the latter the value $4.6 \pm 1.0\%$. Simulations also show that the introduction of anisotropy in the hf interaction would only result in a minor correction (<0.3 on the value 4.6).

The resonance line in the $g = 4$ region is attributed to forbidden $\Delta m = 2$ transitions of the same $S = 1$ or $3/2$ centre: Comparison of the intensities of these $\Delta m = 2$ signals with the allowed $\Delta m = 1$ transitions revealed a close correlation. This is exemplified in figure 3(b), where the ratio of the peak-to-peak height of the $\Delta m = 2$ resonance $h_{pp}^{\Delta m=2}$ to $h_{pp}^{S=1}$ is shown as

a function of the weight normalized $h_{pp}^{S=1}$. Figure 5 compares the shape of simulated $\Delta m = 2$ transition spectra (dotted lines) to experimental half field resonances (solid lines) for both K- and Q-band observations. The simulated spectra were obtained by applying work by De Groot and Van Der Waals [16]. Starting from the Hamiltonian combining the Zeeman and spin–spin term (cf the first two terms in equation (1)), this work presents a detailed calculation scheme for the powder pattern line shape of the $\Delta m = 2$ transitions for paramagnetic $S = 1$ centres with an axial $\hat{D}$ tensor ($E = 0$). A more generalized treatment ($E \neq 0$) is given by Kottis and Lefebvre [17]. Calculations were carried out assuming $D = 358$ G and the parameter ΔB_{pp}^{R} was allowed to vary in order to optimize the fit. This resulted in ΔB_{pp}^{R} values differing significantly for the K- and Q-bands and different from the the previously obtained value for the $\Delta m = 1$ spectrum (1.75 G): for K- and Q-band the values 1.2 ± 0.2 G and 0.6 ± 0.1 G were obtained respectively. In order to increase the signal-to-noise ratio, both experimental spectra shown in figure 5 were obtained by applying relatively high P_{μ} and modulation field amplitude B_{mod}. This may well have distorted and broadened the signal line shape to some degree. Nevertheless, the typical asymmetric line shape signature, as well as the signal peak-to-peak width are in reasonably good agreement with the predictions for $S = 1$. In the $S = 3/2$ case, the $\Delta m = 2$ transition spectra are generally more complicated, as can readily be deduced from the working method outlined in [17]. Typically, a double structure with a separation of the same order as that between the $\Delta m = 1$ lines is expected, centred approximately at half the value of the $\Delta m = 1$ resonance centre [18].

5. Discussion

The difficulty of distinguishing between an $S = 1$ and $S = 3/2$ resonance due to the occurrence of superposed strong central lines originating from other centres has been encountered before in the literature [19]. Yet for the current centre, two elements strongly favour the $S = 1$ interpretation. First, there is the absence of correlation (cf figure 4, inset (C)) between the structure of the central line in the experimental spectrum (full curve) and the central line as obtained from the simulation (dotted curve). The simulations show that, should $S = 3/2$, the central line would be noticeably distorted. For clarity, the signal at $g = 2.004\,30$ is too small to be confused with such an $S = 3/2$ central signal. Moreover, control measurements at the K-band did not exhibit noticeable changes in the structure of the central line. A second argument in favour of the $S = 1$ interpretation is the asymmetric shape, position and the frequency dependent broadening toward the lower ν of the resonance line near $g = 4$. As demonstrated in figure 5 these are in close agreement with the predictions for $S = 1$. Hence we conclude that the newly observed spectrum pertains to an $S = 1$ defect, where it now remains to assess its atomic nature. Obviously, for this purpose the observed hf structure is most informative.

Considering the chemical composition of the samples, only a limited number of elements can be proposed for the occurring 28.3 G hf doublets. Valid candidates for the surrounding nuclei are C atoms, one of the frequent impurities, i.e. H, N, O, ... or the 'CVD dopants' Fe, Ni, Mo, ... Taking into account the nuclear spin of these elements and the natural abundance of their isotopes, together with the 4.6% intensity ratio of the hf lines to the main spectrum, several possible combinations of elements and number of equivalent positions in the defect may be considered. Within experimental error, the intensity ratio would match the occurrence of four equivalent C sites (^{13}C; 1.11% abundant) surrounding the defect. Alternatively, the hf doublets could be attributed to the interaction of a single Si atom (^{29}Si; 4.70% abundant). Finally the hf lines could also be explained as the result of the interaction with two equivalent Fe (^{57}Fe; 2.19% abundant) atoms.

Table 1. ESR parameters of the divacancy (V–V) at 33 K taken from the work by Twitchen *et al* [5], and of the $S = 1$ centre at 293 K reported in this work, obtained by fitting experimental spectra with Hamiltonian (1). n represents the number of nearest and next nearest neighbours. Values in brackets indicate estimated error margins.

Centre	Spin	g_1	g_2	g_3	D (G)	E (G)	n	$A_\parallel$ (G)	$A_\perp$ (G)	ΔB^R_{pp} (G)
V–V	1	2.002 2	2.002 6	2.001 3	166	18.4	4	40.7	20	1.3
							2	4.6	4.6	
Present $S = 1$	1	2.003 86	2.003 86	2.003 86	358	0	4	?	28.3	1.75
centre		(0.000 05)	(0.000 05)	(0.000 05)	(1)	(2)			(0.3)	(0.05)

Also the second observed doublet, of 88 G splitting, could tentatively be ascribed to hf interactions. In this case the intensity ratio of hf lines to the main spectrum is $\sim$14% of 4.6% $\sim$ 0.6%. This ratio matches none of the natural abundance of any feasible present $S = 1/2$ element. However, it could match the natural abundance of ^{61}Ni which has nuclear spin $I = 3/2$ and a natural abundance of 1.19%, if supposing that the two additional lines expected for $I = 3/2$ are masked by the stronger overlapping 28 G hf doublets. The observed hf intensity ratio should then be doubled, i.e. $\sim$1.2%, in good agreement with observations.

6. Interpretation

The inferred fitting parameters for the $S = 1$ centre are compiled in table 1. Also tabulated are the values for the pure divacancy described by Twitchen *et al* [5], which appear similar. Therefore, we shall analyse the microscopic model of the newly observed centre on the basis of a distorted divacancy. In this view, it follows most naturally to attribute the observed hf interaction to the presence of four equivalent NN C atoms. Their presence then suggests a C_{2h} or C_{2v} defect symmetry; T_d symmetry is ruled out because for this high symmetry the term $\boldsymbol{S} \cdot \hat{D} \cdot \boldsymbol{S}$ in the Hamiltonian (1) vanishes. Also, the D_{2d} and D_{2h} symmetries are very improbable in a diamond lattice.

The failure to detect any lines resulting from hf interaction with the next-nearest neighbours in the experimental spectrum is probably because they merge with the central line, given their significantly smaller intensity and splitting. In comparison with the divacancy, the present $S = 1$ centre has the highest values of A and D. The higher value of all A might indicate that the electrons in the $S = 1$ centre are closer to the basal carbon atoms, i.e. the four equivalent atoms surrounding the divacancy. In contrast to the divacancy, the D matrix is perfectly axially symmetric: then, the larger D value for the $S = 1$ centre can be the result of the smaller delocalization of the unpaired electrons.

As expected for a divacancy-like defect, the value of D for the $S = 1$ centre increases linearly with temperature. Indeed, due to the anharmonic character of lattice vibrations, an increase in temperature should cause the basal carbon atoms of a divacancy to move to the unoccupied space, i.e. inwards. This could compress the divacancy leading to an increase in D. Similar variations of D were observed in other (R5, A2) vacancy-like $S = 1$ centres [1]. Furthermore, applying the point dipole approximation [1], the distance between the interacting electrons can be estimated as 4.3 Å, which is close to the spacing between 2 C atoms at opposite sites in a divacancy (3.9 Å).

We suggest that the presence of an impurity is necessary to explain the divacancy distortion in the $S = 1$ centre. This would also explain the remarkable temperature stability of the centre and absence of defect reorientation at room temperature as observed for the divacancy.

Distortion due to intrinsic stress is hardly sufficient to explain the observed temperature stability. In order to conserve the fourfold hyperfine symmetry and the axial $\hat{D}$ symmetry we would situate this impurity inside the vacancy cage. If our interpretation of the second hyperfine doublet is correct, Ni would be a valid candidate.

7. Summary and conclusions

ESR investigation of CVD diamond material has revealed the presence of an undocumented defect centre. On the basis of the specific powder pattern shaped spectrum, the defect is assigned to an $S = 1$ state with $g = 2.003\,86 \pm 0.000\,05$ and an axial spin–spin tensor. The zero-field splitting parameter D is temperature dependent, increasing from 335 G at 10 K to 358 G at room temperature. A major hyperfine structure is attributed to the interaction with four equivalent NN C atoms, while an additionally weak line structure could tentatively be ascribed to a second hyperfine interaction, possibly arising from ^{61}Ni. The centre exhibits a remarkable temperature stability and its occurrence is anticorrelated with the occurrence of the substitutional nitrogen defect.

The defect is interpreted as an impurity stabilized divacancy like defect, the involved impurity possibly being ^{61}Ni. Probably, then, the defect is built in during film deposition as a result of non-ideal CVD processing. It is realized, though, that the advanced 'impurity part' of the model is highly hypothetical, certainly not proven on ESR grounds. More definite conclusions must await further in depth experimenting.

References

[1] Loubser J H N and van Wyk J A 1978 *Rep. Prog. Phys.* **41** 1201
[2] Baker J M and Newton M E 1995 *Appl. Magn. Reson.* **8** 207
[3] Newton M E 1994 *Properties and Growth of Diamond* ed G Davies (London: INSPEC) pp 153–72
[4] van Wyk J A, Tucker O D, Newton M E, Baker J M, Woods G S and Spear P 1995 *Phys. Rev.* B **52** 12 657
[5] Twitchen D J, Newton M E, Baker J M, Anthony T R and Banholzer W F 1999 *Phys. Rev.* B **59** 12 900
[6] Watkins G D and Corbett J W 1965 *Phys. Rev.* A **138** 543
[7] Haque M S, Naseem H A, Shultz J L, Brown W D, Lai S and Gangopadhyay S 1998 *J. Appl. Phys.* **83** 4421
[8] Struck L M and D'Evelyn 1993 *J. Vac. Sci. Technol.* A **11** 1992
[9] Iakoubovskii K, Adriaensens G J and Nesladek M 2000 *J. Phys.: Condens. Matter* **12** 189
[10] Zhou X, Watkins G D, McNamara Rutledge K M, Messmer R P and Chawla S 1996 *Phys. Rev.* B **54** 7881
[11] IMO, Diepenbeek, Belgium
[12] Stesmans A and Van Gorp G 1989 *Rev. Sci. Instrum.* **60** 2949
[13] Van Gorp G and Stesmans A 1992 *Phys. Rev.* B **45** 4344
[14] Weeks R A 1956 *J. Appl. Phys.* **27** 1376
[15] Poole C P 1967 *Electron Spin Resonance: A Comprehensive Treatise on Experimental Techniques* (New York: Wiley–Interscience) p 554
[16] De Groot M S and Van Der Waals J H 1960 *Mol. Phys.* **3** 190
[17] Kottis P and Lefebvre R 1963 *J. Chem. Phys.* **39** 393
[18] Atherton N M 1973 *Electron Spin Resonance: Theory and Applications (Ellis Horwood Series in Physical Chemistry)* (New York: Halsted) p 232
[19] Lomer Jenifer N and Wild A M A 1973 *Radiat. Eff.* **17** 37